Micromechanical evaluation of failure models for unidirectional fiber-reinforced composites

Arefi, Azam; van der Meer, Frans P.; Forouzan, Mohammad Reza; Silani, Mohammad; Salimi, Mahmoud

DOI
10.1177/0021998319867470

Publication date
2019

Document Version
Accepted author manuscript

Published in
Journal of Composite Materials

Citation (APA)
Arefi, A., van der Meer, F. P., Forouzan, M. R., Silani, M., & Salimi, M. (2019). Micromechanical evaluation of failure models for unidirectional fiber-reinforced composites. *Journal of Composite Materials*, *54 (2020)*(6), 791-800. https://doi.org/10.1177/0021998319867470

Full-length research article

Corresponding Author:

Azam Arefi, Isfahan University of Technology, Isfahan, 8415683111, Iran.

Email:a.arefi@tudelft.nl

Micromechanical evaluation of failure models for unidirectional fiber-reinforced composites

Mechanical Engineering

Azam Arefi

Isfahan University of Technology, Isfahan, Iran.

Azam Arefi[1,2], Frans P. van der Meer[2], Mohammad Reza Forouzan[1], Mohammad Silani[1], Mahmoud Salimi[1,3]

[1]Isfahan University of Technology, Department of Mechanical Engineering, Isfahan, 8415683111, Iran

[2]Delft University of Technology, Faculty of Civil Engineering and Geosciences, PO Box 5048, 2600 GA Delft, The Netherlands

[3]University of Alberta, Faculty of Engineering, Edmonton, T6G1H9, Canada

Abstract

In this paper, micromechanical simulations are employed to evaluate the performance of the Tsai-Wu and Hashin failure criteria for fiber-reinforced composites, especially in stress states whose experimental reproduction is complicated. Micromechanical responses are generated using a finite element model of a representative volume element (RVE), in which only the matrix material experiences damage and the fibers are assumed to be elastic. Micromechanical simulations of basic load cases are used to calibrate macrolevel criteria. Finally, the response of the micromodel and macromodels is compared for various load combinations. Despite a good agreement between Tsai-Wu criterion predictions and micromodel results in a wide range of stress states, some stress combinations are highlighted for which the strength is not predicted accurately. Additionally, accuracy of the Hashin criterion suffers from ignoring the influence of stress in fiber direction on matrix failure.

Keywords

Polymer composites, Matrix failure, Micromechanics, Failure criteria.

Introduction

Micromechanical models can be used as a powerful tool for performing virtual mechanical tests. Different loading scenarios that are not easily tested in physical experiments can be simulated for a representative volume element (RVE) of the microstructure. In an RVE, the actual failure and deformation mechanisms of composite materials can be simulated considering appropriate constitutive models for different phases including fiber, matrix and interface, with a limited number of inputs for each phase. For example, micromechanical models have been widely used to generate failure envelopes. Totry et al.[1] employed micromechanical simulations to extract the failure locus of fiber-reinforced composites under transverse compression and out-of-plane shear. Analyses were conducted by simulation of a three-dimensional representative volume element containing fiber, matrix and interface. There was a good agreement between the failure envelopes from micromechanical simulations with those of Puck[2,3] and LaRC[4] failure formulations.

Using the same assumptions, Totry et al.[5] developed a failure envelope for AS4/PEEK composite under transverse compression and longitudinal shear. The validity of the micromechanical results was examined by comparing these results with the predictions of Puck's and LaRC's criteria. The results showed that the Puck criterion estimates failure with adequate accuracy in combined stress states where failure is governed by the matrix material. Moreover, Totry et al.[6] used micromechanical simulations to investigate the effect of the loading path on the failure envelope of unidirectional fiber reinforced composites under transverse compression and shear. The results showed that failure envelopes were independent of the loading path.

Naya et al.[7] employed a computational micromechanics framework to predict ply properties and investigate the effect of microstructure on the homogenized behavior of composites. The failure envelope of unidirectional fiber reinforced composites in longitudinal shear/transverse compression was extracted, considering environmental effects such as humidity and temperature. The results showed that the experimentally observed shear hardening in transverse compression loading is due to the friction between fiber and matrix. It was also concluded that some of the available failure criteria[3, 16] need to be improved to be able to consider the fiber/matrix interface strength and interface friction appropriately.

Recently, the performance of an orthotropic plasticity model for fiber reinforced composites was investigated by comparing the results of this macro-plasticity model with those obtained using computational micromechanics[8]. The results showed that some simplifications in the macro-model such as ignoring the effect of stress in fiber direction on matrix plasticity and using a single constant Poisson's ratio are not justified.

Currently, different failure criteria are available to interpolate strength in general stress space from a limited set of basic strength values[9-13]. Most of these models are phenomenological, i.e. they are inspired by experimental observations and provide relations that allow for accurate fitting of known data sets. Micromechanics allows for evaluating the accuracy of these failure criteria under stress combinations that are not

easily achieved in experiments. While earlier studies based on micromechanical simulations focused on the classical stress combinations to validate the concept, the research presented in this paper uses micromechanical simulations to examine the validity of available failure theories for less standard stress combinations.

In this work, a detailed comparison is made between predictions of failure estimated by two classical macro-mechanical failure criteria (Tsai-Wu[9] and Hashin[10]) and micromechanical simulations. Firstly, the micromodel is built as a statistical representative volume element with random fiber distribution. In the micromodel, a consistent pressure-dependent damage model by the authors[14] is adopted for the matrix material. Fibers are assumed to be elastic and isotropic and perfect bonding between fibers and matrix is assumed. Secondly, the micromodel is utilized to generate inputs for the macromodels by implementing five virtual mechanical tests. Finally, by comparing the failure envelopes from micromechanics with those of Tsai-Wu and Hashin, limitations of the two failure criteria are identified.

Failure criteria formulations

Failure criteria in composite lamina can be classified in two main groups, namely: interactive and mode-dependent failure criteria. Interactive criteria are formulated as a single polynomial or tensorial expression in terms of the material strengths. Although the anisotropic nature of the composites considering different strength coefficients in different directions is taken into account, the non-homogenous nature of the composite is disregarded in the sense that one smooth failure envelope is assumed. Mode-dependent criteria distinguish between different failure modes of fiber failure and matrix failure with separate criteria for the different modes. The mathematical expressions of these criteria are developed in terms of the material strengths.

In this study, the two most popular failure criteria, namely, Tsai-Wu and Hashin failure criteria are used as representative for the categories of interactive and mode-dependent criteria, respectively. These models have been selected because they provide reasonable predictions of damage initiation in composites for various stress combinations.

Tsai-Wu failure criterion

The most general failure criterion for composite materials is the tensor polynomial criterion proposed by Tsai and Wu[9]. This criterion may be expressed in tensor notation as:

$$F_{ij}\sigma_i\sigma_j + F_i\sigma_i = 1 \tag{1}$$

where Voigt notation is used for the stress. F_{ij} and F_i are a second order tensor and a vector containing the strength values of the material.

Considering the symmetries of the transversely isotropic materials and also the fact that failure of the material is insensitive to the change of sign in shear stresses, Eq. (1) for these materials can be simplified as:

$$\{\sigma_i\}^T.\begin{bmatrix} F_{11} & F_{12} & F_{12} & 0 & 0 & 0 \\ & F_{22} & F_{23} & 0 & 0 & 0 \\ & & F_{22} & 0 & 0 & 0 \\ & & & F_{44} & 0 & 0 \\ & sym & & & F_{55} & 0 \\ & & & & & F_{55} \end{bmatrix}.\{\sigma_i\}+\{\sigma_i\}^T.\begin{bmatrix} F_1 \\ F_2 \\ F_2 \\ 0 \\ 0 \\ 0 \end{bmatrix}=1 \quad (2)$$

In which different parameters are defined as:

$$F_1=\frac{1}{X_T}-\frac{1}{X_C},\ F_2=F_3=\frac{1}{Y_T}-\frac{1}{Y_C},\ F_{11}=\frac{1}{X_T X_C},F_{22}=F_{33}=\frac{1}{Y_T Y_C} \quad (3)$$

$$F_{23}=\frac{1}{2Y_{BT}{}^2}(1-2Y_{BT}F_2-2Y_{BT}{}^2F_{22}),\ F_{44}=\frac{1}{S_T S_T},F_{55}=F_{66}=\frac{1}{S_L S_L}$$

where X_T and X_C are the tensile and compressive longitudinal strengths, respectively, Y_T and Y_C denote the tensile and compressive transverse strengths, Y_{BT} is the biaxial strength and S_T and S_L are the transverse and longitudinal shear strengths, respectively.

Hashin failure criterion

In 1980, Hashin[10] proposed a matrix failure criterion based on the Mohr-Coulomb hypothesis where the fracture will only be influenced by the stresses acting on its plane. This formulation has been developed based on the assumption that failure occurs due to the interaction between different stress components acting on a fracture plane parallel to the fibers. The criterion for matrix tensile failure is defined as:

$$\frac{1}{Y_T^2}(\sigma_{22}+\sigma_{33})^2+\frac{1}{S_T^2}(\sigma_{23}^2-\sigma_{22}\sigma_{33})+\frac{1}{S_L^2}(\sigma_{12}^2+\sigma_{13}^2)^2=1 \quad (4)$$

The Hashin criterion is simple, although its accuracy is limited[15, 16].

Micromechanical simulations

Creation of failure envelopes corresponding to these macroscopic failure criteria requires some strength parameters as inputs which can be obtained from experimental measurements. In this work, micromechanical simulations of RVEs are used to extract inputs for these criteria. In the micromodel, glass fibers are assumed to be elastic and isotropic with Young's modulus of 74000 MPa and Poisson's ratio of 0.2[17]. A consistent pressure-dependent damage model[14] is adopted to simulate the matrix material behavior. In this model, the constitutive behavior of the matrix material is governed by:

$$\boldsymbol{\sigma}=(1-d)\mathbf{C}_0\boldsymbol{\varepsilon}^e \quad (5)$$

with $\mathbf{C}_0$ being the elastic stiffness tensor and d being the damage parameter defined as:

$$d=\frac{\varepsilon^f(\varepsilon_{eq}-\varepsilon^0)}{\varepsilon_{eq}(\varepsilon^f-\varepsilon^0)} \quad (6)$$

where ε^0 and ε^f are the uniaxial strain values that correspond to onset and completion of the softening failure process, respectively. The equivalent strain ε_{eq} is a scalar measure derived from the strain tensor and defined as:

$$\varepsilon_{eq} = \frac{-q + \sqrt{q^2 - 4pu}}{2p} \tag{7}$$

with

$$q = 2a(1-a)b\varepsilon^f + (1+2a)c,\ p = b(1-a)^2,\ u = b(a\varepsilon^f)^2 - 2ac\varepsilon^f - rX_cX_t \tag{8}$$

$$a = \frac{\nu X_t}{E(\varepsilon^f - \varepsilon^0)},\ b = \left(\frac{E}{1+\nu}\right)^2,\ c = \left(\frac{E}{1-2\nu}\right)(X_c - X_t)$$

in which, E and ν are the Young's modulus and the Poisson's ratio and X_t and X_c denote to the tensile and compressive strengths, respectively.
Damage grows when the following criterion is met:

$$\varepsilon_{eq} - \kappa \geq 0 \tag{9}$$

where κ is a scalar measure of the largest previously reached equivalent strain level that controls the evolution of the damage surface. For further details of the damage model, the reader is referred to the paper where it has been introduced[14]. A user material subroutine (UMAT) for Abaqus has been implemented in FORTRAN to implement this damage model. The material properties for the epoxy matrix are reported in Table 1.

Table 1. Material properties of epoxy resin[18]

Parameter	Value
Young's Modulus (E)	3760 MPa
Poisson's ratio (ν)	0.39
Tensile strength (X_t)	93 MPa
Compressive strength (X_c)	124 MPa
Mode I fracture toughness	0.09 N/mm

RVE size study

For micromechanical analysis of composites, a representative volume element should be constructed such that the homogenized behavior of RVE represents the macroscopic behavior of the composite. Many different studies considering various formulations for each phase have been conducted to determine the suitable size of RVE in different loading conditions. Recently, a statistical study into the influence of the RVE size on the elasto/plastic response was performed with a large number of different RVEs

of different sizes by van der Meer[8]. It was shown that an RVE including 25 fibers is adequate to represent the macroscopic material under longitudinal shear and transverse tension loadings. To investigate whether this RVE size is also suitable when damage is included, various RVEs including 25, 36, 49 and 64 fibers were considered and five different fiber realizations for each one were constructed. Glass fibers with a diameter of 5 μm were randomly distributed inside the periodic RVE with a fiber volume fraction of 60%. Linear wedge elements were used to discretize the models. Figure 1 shows five different realizations and their finite element discretization for RVEs including 25 fibers. Periodic boundary conditions were applied to the RVEs following van der Meer[8]. These boundary conditions were imposed as linear multipoint constraint equations for each nodal pair using a python script.

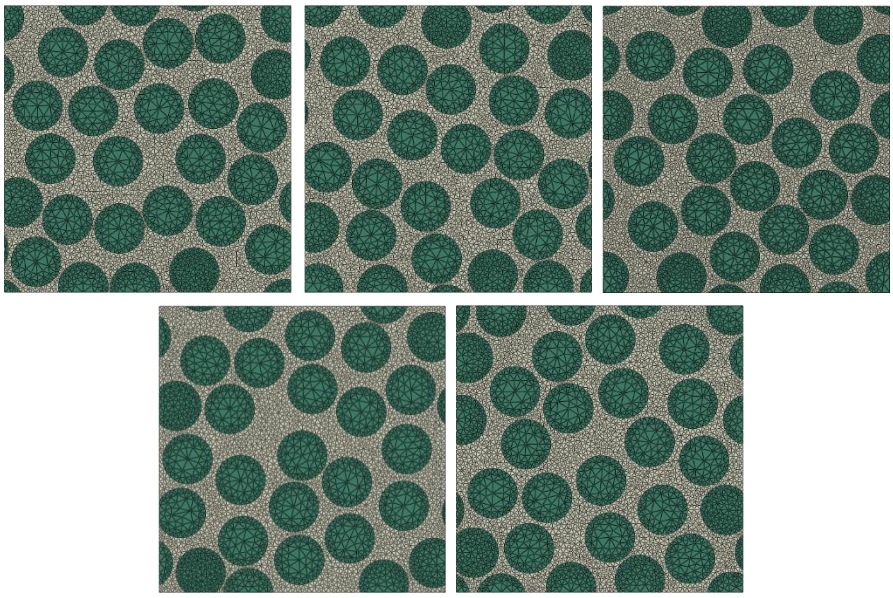

Figure 1. Five realizations of a fiber distribution with 25 fibers and their finite element discretization.

Finally, the homogenized stress-strain curves were obtained using the following definitions for averaged stresses and strains over the RVE volume

$$\boldsymbol{\sigma} = \frac{1}{V}\int_V \boldsymbol{\sigma} dV \,, \quad \boldsymbol{\varepsilon} = \frac{1}{V}\int_V \boldsymbol{\varepsilon} dV \tag{10}$$

which were implemented via a python script in the post-processing mode in Abaqus. A statistical study is performed into the influence of RVE size on different strength values by performing virtual tests for four different RVE sizes from 25 fibers to 64 fibers with five different realizations for each RVE size. The mean and standard deviation of the resulting strength values are plotted in Figure 2. It can be seen that the average strength for the different load cases is approximately constant and does not change when the RVE

size increases. Therefore, the composite strength in basic load cases is considered to be equal to the average from five RVEs with 25 fibers. However, it was found that for combined loading, the variation in the response increased (Figure 3). For this reason, for cases where the interaction between three different stress components is studied, the results are extracted from simulations of two RVEs with 64 fibers.

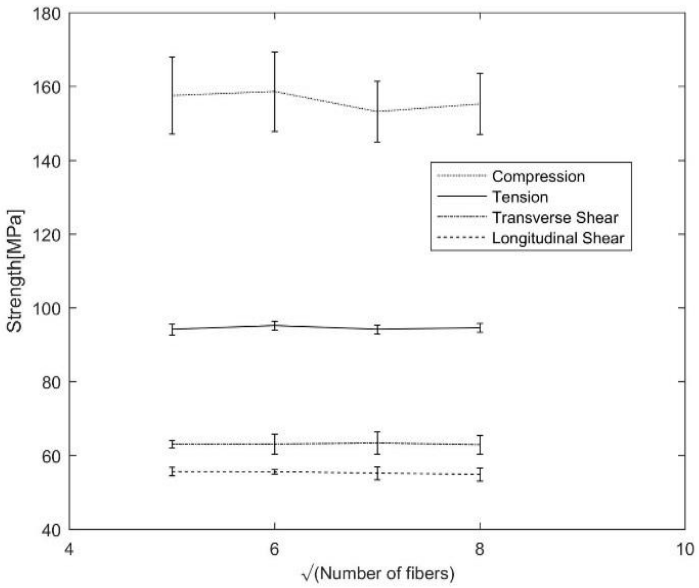

Figure 2. Mean and standard deviation of tensile, compressive, longitudinal shear and transverse shear strengths for 5 realizations for various RVE sizes.

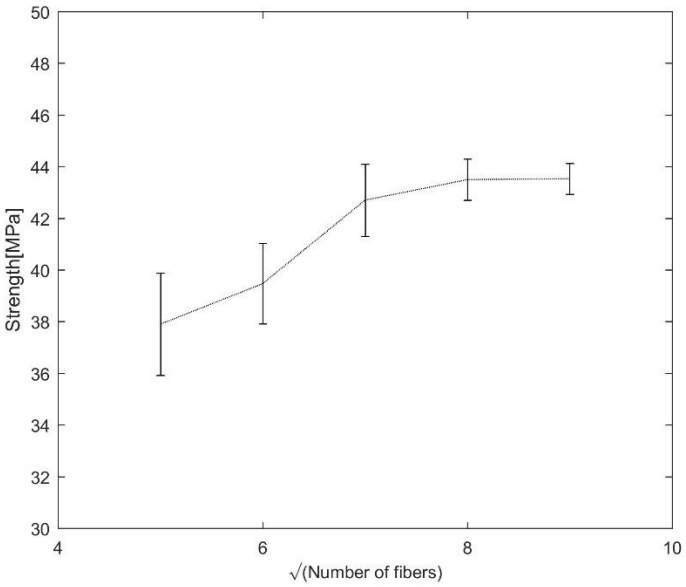

Figure 3. Mean and standard deviation of maximum longitudinal shear stress for 5 realizations for various RVE sizes in combined loading including longitudinal tension and longitudinal shear in two different planes.

Results

Five basic load cases (uniaxial and biaxial tension, uniaxial compression, and transverse and longitudinal shear) are applied to the RVEs and the relevant strength values are computed. Next, the response of the macroscopic models is compared with those of the micromodel for a wide range of stress combinations. Simulations are carried out with different displacement ratios corresponding to different loading combinations. The failure envelopes corresponding to the micromodel are extracted based on the assumption that under different stress states the failure occurs when the maximum homogenized normal or shear stress in the RVE is attained. For example, to extract the failure envelope in $\sigma_{13}-\sigma_{12}$ stress space, the homogenized $\sigma_{13}-\sigma_{12}$ curves extracted by applying different δ_{13}/δ_{12} ratios on an RVE were obtained and plotted in Figure 4(a). Following literature[5,6], the failure point is identified by finding the maximum value in one of the stress components, in this case the maximum σ_{12} value. Figure 4(b) represents the damage distribution in the micromodel at the peak under this load combination for $\delta_{13}/\delta_{12}=1$.

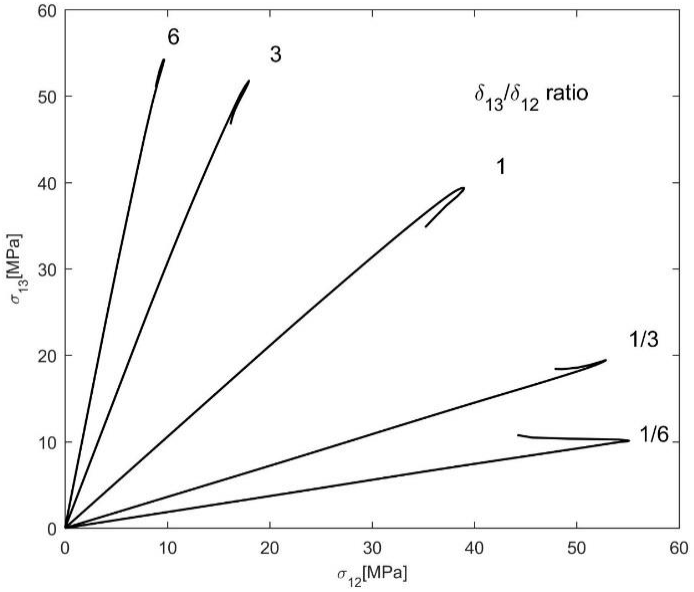

(a)

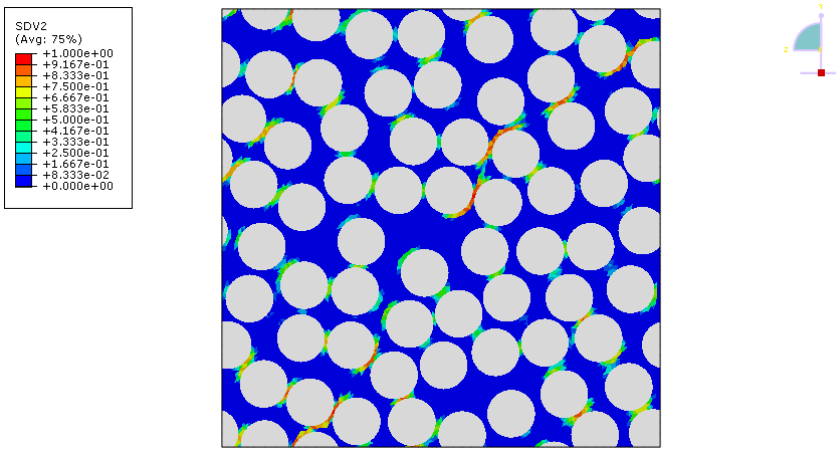

(b)

Figure 4. (a) Mechanical response of the composite under biaxial deformation in the $\sigma_{12}-\sigma_{13}$ stress space. (b) Damage distribution in the micromodel at the peak under $\sigma_{12}-\sigma_{13}$ combined loading for $\delta_{13}/\delta_{12}=1$.

Since in the micromodel no damage is considered for the fibers, only matrix failure will be observed. Consequently, in combined loadings including loading in fiber direction, failure envelopes will remain open.

Calibration

The strength parameters computed using micromechanical simulations of five RVEs including 25 fibers are summarized as: $Y_T=94.2\,\text{MPa}$, $Y_C=155\,\text{MPa}$, $S_T=63\,\text{MPa}$, $S_L=55.7\,\text{MPa}$.

In the Tsai-Wu criterion in some kinds of loadings the longitudinal strengths are also needed as inputs. However, these values cannot be computed through the current micromodel because the fiber failure is not included. Therefore, these values are extracted from available data in the literature. The longitudinal tensile and compressive strengths are set equal to 1280 Mpa and 800 MPa[17], respectively.

Matrix-dominated stress combinations

Longitudinal shear/longitudinal shear envelope

In this section, the interaction between longitudinal shear stresses in different planes is studied. In Figure 5 the failure envelope in $\sigma_{12}-\sigma_{13}$ plane is visualized. The values are obtained by averaging from two different realizations. It can be seen that the Tsai-Wu and Hashin failure criteria are completely coincident in this plane. There is a very good match between the micromechanical results with the macro ones which means that the interaction between these two stress components is well captured using the macro failure criteria.

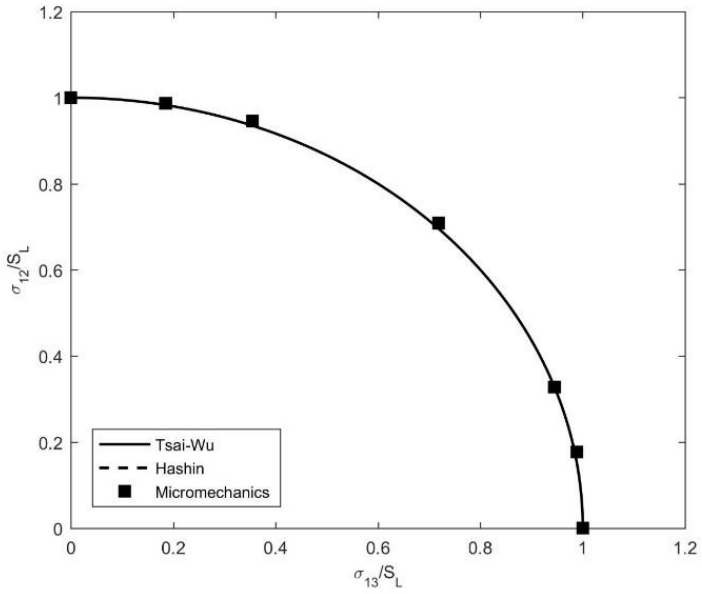

Figure 5. Stress envelope for combined longitudinal shear in two different planes.

Longitudinal shear/transverse tension

To investigate the interaction between longitudinal shear and transverse tension, two different load combinations are considered: one where the shear and tension act in the same plane and one where they act in two different planes (see Figure 6).

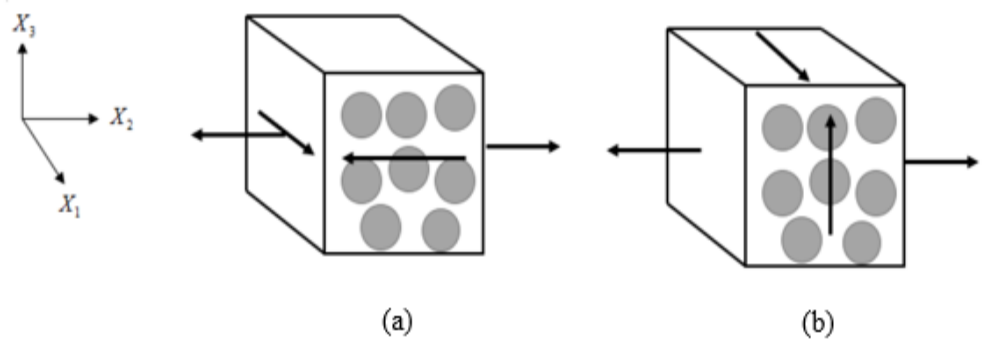

Figure 6. Combination of transverse normal stress with longitudinal shear stress applied (a) in the same plane, (b) in two different planes.

Micromodel results corresponding to these load combinations are plotted in Figure 7. The results show that by applying transverse tension and longitudinal shear at the same plane, failure occurs faster than applying these loads in different planes. These observations can be explained by looking at the microscopic failure mechanisms. In the load case of Figure 6(b), the microscopic shear stress concentrations are not located at the

same position as the microscopic tensile stress concentration. As a consequence, little interaction between the different macroscopic stresses is found. The distinction between the two load cases in Figure 7 cannot be found in the macroscopic failure criteria.

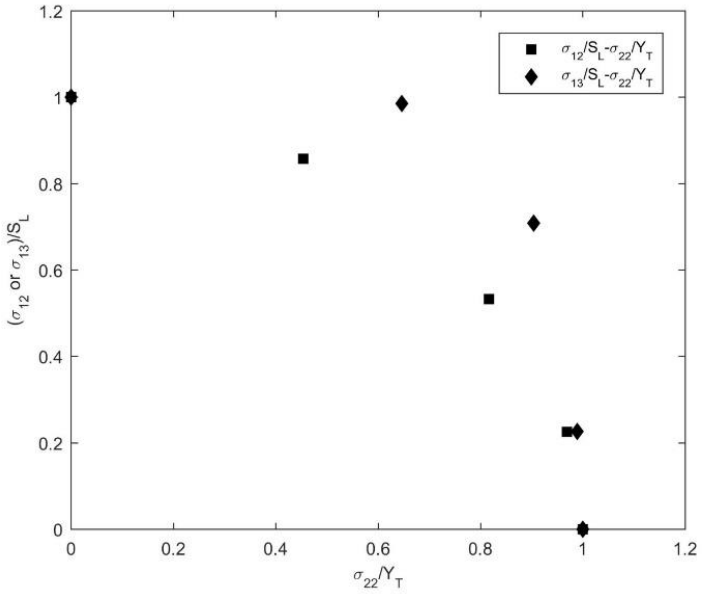

Figure 7. Stress envelopes for different combinations of longitudinal shear stresses with transverse normal stress.

Transverse biaxial tension envelope in presence of longitudinal shear

Next, a combination of three different stress components is investigated. A constant longitudinal shear stress σ_{12} is applied along with increasing transverse loads σ_{22} and σ_{33} achieved by applying increasing displacements on the corner nodes with fixed ratio δ_{22}/δ_{33}. The results for this load combination are shown in Figure 8 in which the point corresponding to maximum σ_{22} is considered as the failure point for each displacement ratio. In this figure, for low ratios of shear stresses ($\sigma_{12}/S_L = 0, 0.2$), Tsai-Wu and micromodel have the same predictions of the failure stress and the curves are symmetric with respect to the $\sigma_{22} - \sigma_{33} = 0$ axis. It should be noted that for calculation of the Tsai-Wu criterion under combined σ_{22} and σ_{33} stresses, the biaxial transverse strength of the composite determined by micromechanical simulation is substituted into Eq. (3). For higher values of σ_{12}/S_L, the Tsai-Wu failure envelope keeps its symmetry. However, the micromodel does not. A higher failure stress is found in the region in which $\sigma_{33} > \sigma_{22}$. The micromodel predicts that interaction between σ_{12} and σ_{33} is limited, in contrast with interaction between σ_{12} and σ_{22}. These results are in line with the previous observations in section 4.2.2.

The high discrepancy between Hashin estimation of the stress envelope from micromechanics is related to the fact that the biaxial tensile strength does not appear in

the criterion formulation. Therefore, the Hashin failure envelope has less freedom to be fitted with the micromodel results in this plane. Considering the point of failure where $\sigma_{22} = \sigma_{33}$, Eq. (4) yields:

$$Y_{BT} = \frac{Y_T S_T}{\sqrt{4S_T^2 - Y_T^2}} \tag{11}$$

For the considered material, Eq. (11) results in $Y_{BT} = 70.92\,\text{MPa}$, which is significantly different from the micromechanics prediction of $Y_{BT} = 100.4\,\text{MPa}$.

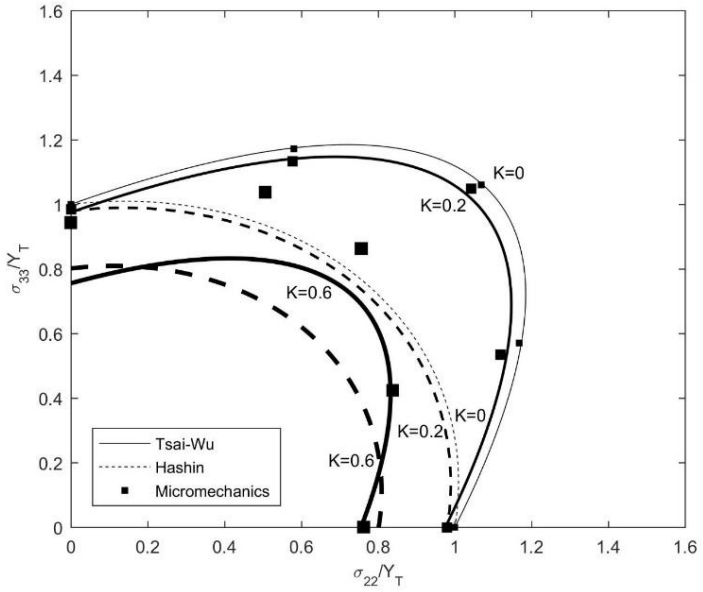

Figure 8. Failure surface of the composite subjected to biaxial transverse tension and longitudinal shear ($K = \sigma_{12} / S_L$).

Effect of stress in fiber direction on failure

In mode-dependent failure criteria such as Hashin in which the fiber and matrix failure modes are separated, the stress in the fiber direction does not have any influence on the failure stress in the matrix failure modes. However, loading in fiber direction does affect the stress state in the matrix and can therefore be expected to have some effect on the matrix failure behavior. To investigate this effect, micromechanical simulations are performed for two different loading combinations: longitudinal shear and fiber tension and transverse tension and fiber tension. The simulations have been done for these stress combinations in presence of various constant values for other stress components.

Longitudinal tension/longitudinal shear envelope

By simplifying the Tsai-Wu criterion in longitudinal tension/longitudinal shear loading, it can be seen that the maximum longitudinal shear stress is defined as a quadratic function of σ_{11}, while in the Hashin criterion, the maximum longitudinal shear stress is independent of the stress in fiber direction.

To extract micromechanics-based failure envelopes simulations were carried out with a fixed ratio of the shear displacement δ_{12} to the normal displacement δ_{11} for different constant values of σ_{13}. The resulting envelopes are shown in Figure 9. All curves related to the Hashin criterion are straight lines as the shear response is completely independent of the longitudinal stress, while micromechanical results show a clear influence of longitudinal stress on the shear strength. It can be seen that the presence of tensile stress in fiber direction reduces the longitudinal shear strength. By contrast, there is a good match between the stress envelope from micromechanics and the Tsai-Wu failure criterion.

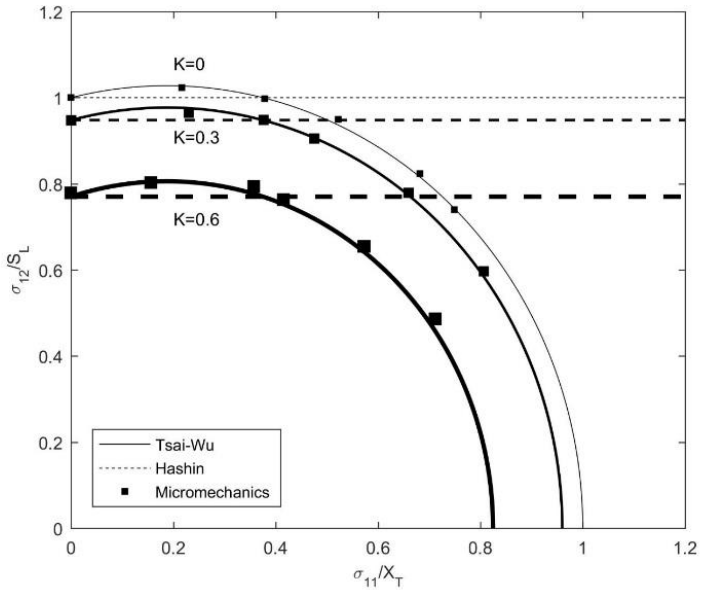

Figure 9. Variation of longitudinal shear strength with respect to the longitudinal axial tension for various $K = \sigma_{13} / S_L$ ratios.

Longitudinal tension/longitudinal shear envelope in presence of transverse shear

Figure 10 shows the failure envelopes corresponding to the Tsai-Wu and Hashin criteria in comparison with micromechanical results in σ_{11}, σ_{12} and σ_{23} loading . It can be seen that the variation of longitudinal shear strength with fiber tensile loading for various σ_{23} / S_T ratios follows the same trends as the previous load combination.

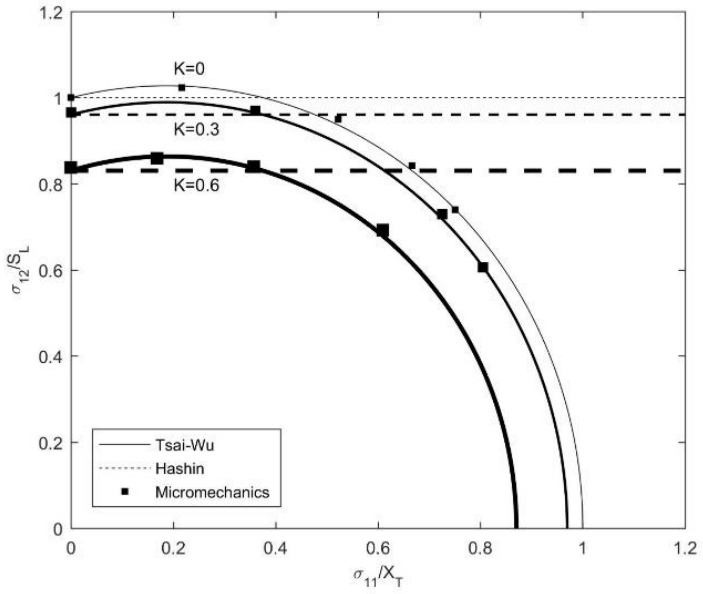

Figure 10. Stress envelope for combined longitudinal shear and fiber tension loadings for various $K = \sigma_{23} / S_T$ ratios.

Longitudinal tension/longitudinal shear envelope in presence of transverse tension

For a multi-axial stress combination including longitudinal/transverse tension and longitudinal shear stress, Eq. (2) becomes:

$$F_{11}\sigma_{11}^2 + F_1\sigma_{11} + F_{22}\sigma_{22}^2 + F_2\sigma_{22} + 2F_{12}\sigma_{11}\sigma_{22} + F_{55}\sigma_{12}^2 = 1 \qquad (12)$$

In Eq. (12), F_{12} determines the interaction between normal stresses in fiber direction and in transverse direction. In order to find this parameter, it is necessary to use a biaxial test involving both σ_{11} and σ_{22}. Different values for F_{12} have been proposed in literature[19-22]. Among those values, the best fit between micromodel results and the Tsai-Wu envelope was obtained for F_{12}=0. Therefore, F_{12} is set equal to zero for the following visualization.

Figure 11 shows the failure envelopes relating σ_{12} with σ_{11} for different values of the normal stress σ_{22}. It is observed that by increasing transverse tensile loading, the longitudinal shear strength decreases considerably. This observation is physically expected. Considering that σ_{12} and σ_{22} have the same action plane, the presence of σ_{22} will accelerate failure due to σ_{12}. Again, a significant influence of σ_{11} on matrix failure is found in the simulations, which is in agreement with the Tsai-Wu criterion but not with the Hashin criterion.

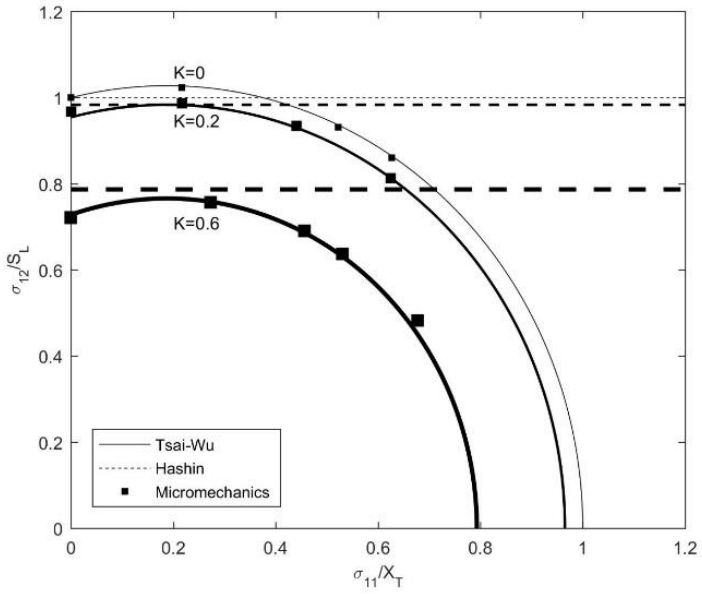

Figure 11. Longitudinal shear strength as a function of σ_{11} for different values of normal stress ratios ($K = \sigma_{22} / Y_T$).

Longitudinal/transverse tension envelope in presence of transverse shear

Additional simulations are performed for a combination of σ_{11} and σ_{22} at constant σ_{23}. The results shown in Figure 12 are similar to those for longitudinal shear in combination with longitudinal tension and transverse shear (Figure 10).

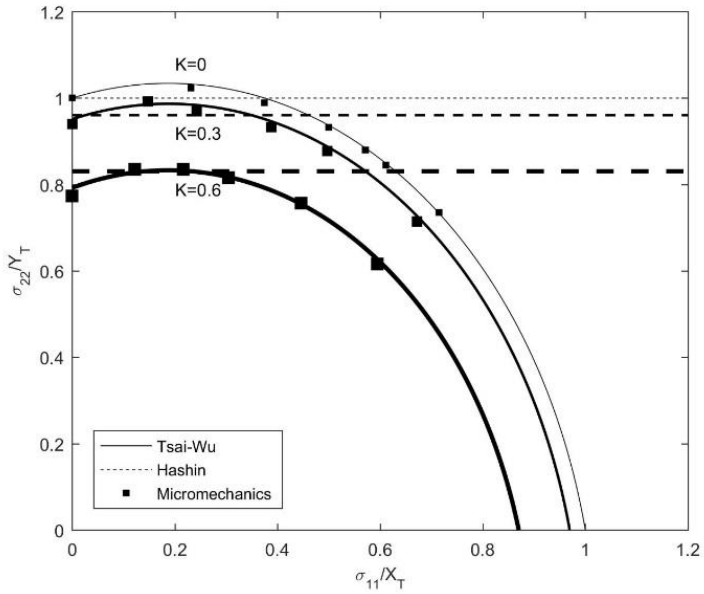

Figure 12. $\sigma_{22} - \sigma_{11}$ Failure envelope accompanied with transverse shear stress ($K = \sigma_{23} / S_T$).

Again, stress in fiber direction accelerates matrix failure. The presence of transverse shear stress results in a shrinkage of the stress envelope.

Conclusion

In this paper, computational micromechanics was employed to examine the performance of macroscopic failure criteria in several multi-axial stress states. The failure criteria were calibrated with the results of RVEs including 25 elastic fibers and a pressure-dependent damaging matrix in four basic virtual mechanical tests. Various stress combinations were applied to the RVE using periodic boundary conditions and the failure envelopes from micromechanics were compared with those of the Tsai-Wu and Hashin failure criteria. Considering the failure envelopes obtained for longitudinal shear/longitudinal tension and also transverse tension/longitudinal tension, it was found that the stress in fiber direction has a significant effect on the predicted failure load. Although this effect is taken into account in the Tsai-Wu criterion, it is left out of consideration in the Hashin criterion. Other failure-mode based failure criteria (Puck[2,3], LaRC[4] and Camanho[11]) suffer the same shortcomings as Hashin for the presented stress combinations.

A significant difference was found between the predictions of the two macroscopic failure criteria and micromodel response in combined loadings including transverse tension and longitudinal shear. According to the micromodel, the interaction between these two stress components depends on whether they are in the same plane or not. The failure criteria do not support making this distinction.

In biaxial transverse tensile loading, there was a good correlation between the failure envelopes from micromechanics and that of Tsai-Wu, whereas, because of the absence of the biaxial transverse strength in the Hashin criterion, an improper estimation of the failure in biaxial transverse stress space was observed.

References

1. Totry E, Gonzalez C, LLorca J. Failure locus of fiber-reinforced composites under transverse compression and out-of-plane shear. Compos Sci Technol 2008; 68:829-839. https://doi.org/10.1016/j.compscitech.2007.08.023.

2. Puck A, Schürmann H. Failure analysis of FRP laminates by means of physically based phenomenological models. Compos Sci Technol 1998; 58:1045–1067. https://doi.org/10.1016/S0266-3538(96)00140-6.

3. Puck A, Schürmann H. Failure analysis of FRP laminates by means of physically based phenomenological models. Compos Sci Technol 2002; 62:1633–1662. https://doi.org/10.1016/S0266-3538(01)00208-1.

4. Pinho ST, Dávila CG, Camanho PP, Iannucci L, Robinson L. Failure Models and Criteria for FRP Under In-Plane or Three-Dimensional Stress States Including Shear Non-Linearity. NASA Langley Research Center, Hampton, Technical Report, 2005.

5. Totry E, Gonzalez C, LLorca J. Prediction of the failure locus of C/PEEK composites under transverse compression and longitudinal shear through computational micromechanics. Compos Sci Technol 2008; 68:3128–3136. https://doi.org/10.1016/j.compscitech.2008.07.011.

6. Totry E, Gonzalez C, LLorca J. Influence of the loading path on the strength of fiber reinforced composites subjected to transverse compression and shear. Int J Solids Struct 2008; 45:1663–1675. https://doi.org/10.1016/j.ijsolstr.2007.10.014.

7. Naya F, Gonzalez C, Lopes CS, Van der Veen S, Pons F. Computational micro-mechanics of the transverse and shear behavior of unidirectional fiber reinforced polymers including environmental effects. Compos Part A Appl Sci Manuf 2017; 92:146-157. https://doi.org/10.1016/j.compositesa.2016.06.018.

8. van der Meer FP. Micromechanical validation of a mesomodel for plasticity in composites. Eur J Mech A-SOLID 2016; 60:58-69. http://dx.doi.org/10.1016/j.euromechsol.2016.06.008.

9. Tsai SW, Wu EM. A general theory of strength for anisotropic materials. J Compo Mater 1971; 5:58-80. https://doi.org/10.1016/j.euromechsol.2016.06.008.

10. Hashin Z. Failure criteria for unidirectional fiber composites. J Appl Mech 1980; 47:329-334. doi:10.1115/1.3153664.

11. Camanho PP, Arteiro A, Melro AR, Catalanotti G, Vogler M. Three-dimensional invariant-based failure criteria for fibre-reinforced composites. Int J Solids Struct 2015; 55:92–107. https://doi.org/10.1016/j.ijsolstr.2014.03.038.

12. Catalanotti G, Camanho PP, Marques AT. Three dimensional failure criteria for fiber-reinforced laminates, Compos Struct 2013; 95: 63-79. https://doi.org/10.1016/j.compstruct.2012.07.016.

13. Sun CT, Tao JX. Prediction of failure envelopes and stress strain behaviors of composite laminates, Compos Sci Technol 1998; 58:1125-1136. https://doi.org/10.1016/S0266-3538(01)00211-1.

14. Arefi A, van der Meer FP, Forouzan MR, Silani M. Formulation of a consistent pressure-dependent damage model with fracture energy as input. Compos Struct 2018; 201:208-216. https://doi.org/10.1016/j.compstruct.2018.06.005.

15. Icardi U, Locatto S, Longo A. Assessment of Recent Theories for Predicting Failure of Composite Laminates. Appl Mech Reviews 2007; 60:76-86. doi:10.1115/1.2515639.

16. Davila C, Camanho PP, Rose CA. Failure criteria for FRP laminates, J Compos Mater 2005; 39:323-345. https://doi.org/10.1177/0021998305046452.

17. Soden PD, Hinton MJ, Kaddour AS. Lamina properties, lay-up configurations and loading conditions for a range of fibre-reinforced composite laminates. Compos Sci Technol 1998; 58:1011-1022. https://doi.org/10.1016/S0266-3538(98)00078-5.

18. Melro AR, Camanho PP, Andrade Pires FM, Pinho ST. Micromechanical analysis of polymer composites reinforced by unidirectional fibres: Part I – constitutive, constitutive modelling. Int J Solids Struct 2013; 50:1897-1905. https://doi.org/10.1016/j.ijsolstr.2013.02.009

19. Tsai SW. A survey of macroscopic failure criteria for composite materials. J Reinf Plas Compos 1984; 3:40–62. https://doi.org/10.1177/073168448400300102.

20. Tsai SW, Hahn HT. Introduction to composite materials. Westport: Technomic, 1980.

21. Deteresa SJ, Larsen GJ. Derived interaction parameters for the Tsai-Wu tensor polynomial theory of strength for composite materials. In: 2001 American society of mechanical engineers international mechanical engineering congress & exposition, New York, N.Y.; November 11–16, 2001.

22. Shuguang L, Sitnikova E., Yuning L., Abdul-Salam K. The Tsai-Wu failure criterion rationalized in the context of UD Composites. Compos Part A 2017; 102:207–217. https://doi.org/10.1016/j.compositesa.2017.08.007.